Rational design of small-molecule peptidomimetics for three pivotal protein secondary structures

Jeong Yeon Yoo,[a] Chanwoo Kim,[a] Ji Hoon Kwon,[a] Hana Cho,[a] Kiyoung Jeong, [a] Wonwoo Park,[a] Younghun Kim,[b] Dongwhan Lee,[b] and Seung Bum Park*,[a]

[a] J. Y. Yoo, Dr. C. Kim, J. H. Kwon, Dr. H. Cho, K. Jeong, W. Park, and Prof. Dr. S. B. Park.
CRI Center for Chemical Proteomics, Department of Chemistry, Seoul National University
Seoul 08826 (Korea)
E-mail: sbpark@snu.ac.kr

[b] Y.Kim and Prof. Dr. D. Lee
Department of Chemistry, Seoul National University
Seoul 08826 (Korea)

Abstract: In the pursuit of modulating protein-protein interactions (PPIs) using small molecules, the lack of studies addressing PPI modulation without structural information presents a significant hurdle. Although peptides have been utilized for this purpose, challenges such as permeability and stability persist, emphasizing the necessity for innovative small-molecule modulators. To target unexplored PPIs, we introduced a computational method encompassing three essential secondary structures of peptidomimetic scaffolds—α-helix, β-strand, and β-turn—serving as key recognition motifs for protein-protein interfaces. These scaffolds (**1**–**3**), systematically derived from a single pyrimidodiazepine skeleton, demonstrated precise alignment with each secondary structure, validated through *in-silico* analysis and X-ray crystallography. Subsequently, our pyrimidine-containing peptidomimetic scaffolds underwent rigorous evaluation *via* diverse phenotypic screenings. Positioned as invaluable chemical tools, these scaffolds hold immense potential for discovering novel PPI modulators. Our design strategy offers a rational approach, overcoming the inherent pharmacokinetic and pharmacodynamic limitations of traditional peptides. By leveraging structures and drug-like properties of small molecules, we aim to pioneer a new era in the design and synthesis of effective PPI modulators.

Proteins, while inherently functional on their own, often exert their biological influence through intricate interactions with other proteins. These protein-protein interactions (PPIs) orchestrate the complex molecular choreography that underpins fundamental cellular processes, shaping the proper functioning of biological systems[1]. Over the past two decades, the scientific community has increasingly focused on PPIs as a novel category of therapeutic targets, driven by advancements in understanding their dynamic nature[2]. The approval of PPI

drugs such as Venetoclax (2016) and Tafamidis (2019) marked a transformative shift, dispelling the notion that PPIs were once considered undruggable[3]. Simultaneously, targeted protein degradation (TPD) has emerged as a revolutionary modality in drug discovery, with PROTAC (PROteolysis TArgeting Chimeras) leading the charge[4]. PROTAC induces interaction between a protein of interest and its E3 ubiquitin ligase, resulting in ubiquitination and subsequent proteasome-mediated degradation of the target protein[5]. This groundbreaking technology selectively eliminates disease-causing proteins by harnessing the cellular recycling machinery. In contrast, our group introduced targeted protein upregulation (TPU), which entails the selective upregulation of disease-fighting proteins by inhibiting PPI between the protein of interest and its E3 ligase[6]. The success of PROTAC and related proximity-induced regulations hinges on a profound comprehension of PPIs' dynamic and context-dependent nature, which governs cellular protein homeostasis and provides a new strategy for selectively modulating cellular processes.

Despite the significance of PPIs, a universal design strategy for modulating unexploited PPIs remains elusive, challenging conventional rational design approaches[1]. PPI interfaces lack distinct binding cavities, unlike traditional druggable targets with discrete binding pockets[1,7]. PPI interfaces typically have a large surface area (1500~3000 Å), much larger than the ligand contact area, and are generally flat without pockets or grooves. Since PPI interfaces are not always continuous, it is difficult for small molecules to mimic the original partner protein. Therefore, discovering PPI modulators necessitates exclusive design strategies relying on structural information due to the unique properties of PPIs. Only about 60 PPIs have been targeted in the human interactome, estimated to have more than 650,000 interactions, and there are only six FDA-approved small-molecule PPI drugs to date[1,8,9] (**Figure 1A**). Modulators targeting PPIs can be classified into peptides, antibodies, and small molecules, with peptides and antibodies being commonly reported[10]. However, peptides and antibodies still suffer from their inherent drawbacks, which include limited stability towards proteolysis, poor cell permeability, and pharmacokinetics. Therefore, developing small-molecule-based PPI modulators with drug-like properties is crucial.

Addressing the challenges of modulating PPIs with small molecules, attributed to their unique interfaces, necessitates recognizing the significance of "hot spots" within these interfaces[11] (**Figure 1B**). Hot spots represent interface residues that most significantly contribute to PPI binding affinity, with alanine scanning mutagenesis often resulting in a Gibbs free energy increase of over 2 kcal/mol[12]. Comprising approximately 10% of the protein interfaces, these identified hot spots predominantly influence protein binding events[13]. While PPI interfaces typically present vast and intricate challenges for small molecules, targeting

these concentrated hot spots can be a promising avenue for effective PPI modulation with small molecules[11]. This delicate approach holds potential for advancing drug development strategies and exploring undeveloped opportunities in the realm of protein-protein interactions.

The major secondary structures governing PPIs—α-helix, β-strand, and β-turn—collectively constitute over 90% of the protein interfaces[1,13]. These secondary structures provide fundamental frameworks for organizing hot spots within proteins[13]. While mimicking these structures with small-molecule scaffolds has shown promise[14], previous structures have often comprised repetitions of units with limited drug-likeness (**Figure 2A**), requiring varied synthetic strategies to mimic the diverse secondary structures of target proteins[15–23]. Traditional design approaches have proven cumbersome and hindered targeted intervention across numerous PPIs.

To overcome inherent limitations in previous peptidomimetic scaffold designs, our study aimed to devise novel scaffolds systematically derived from a single privileged substructure with high biological relevance, capable of mimicking three pivotal protein secondary structures as part of our ongoing pursuit for molecular diversity[24,25]. This endeavor led us to explore the potential of generating multiple scaffolds from pyrimidodiazepine—a well-known privileged heterobicycle renowned for its high drug-likeness—as a common moiety[25–27]. The pyrimidodiazepine structure, characterized by a flat aromatic pyrimidine ring and a sp^3-carbon-rich diazepine ring, allows for structural modifications facilitating diverse conformational adaptations[25]. With its 7-membered diazepine ring offering geometrical flexibility and appropriate synthetic modifications, diverse peptidomimetic scaffolds for modulating various PPIs can be constructed. Furthermore, the nitrogen-rich core skeleton of pyrimidodiazepine permits subsequent decoration with hydrophobic residues such as phenylalanine (Phe), leucine (Leu), and tryptophan (Trp) to mimic the hydrophobic PPI interfaces while maintaining the resulting molecules' drug-like properties ($4 \leq \text{cLogP} \leq 6$)[28]. Thus, pyrimidodiazepine-based peptidomimetics scaffolds accommodate hydrophobic substituents for PPI modulation without significantly elevating the overall hydrophobicity of the resultant molecules (**Figure 2B**).

Results and discussion

Rational design of pyrimidine-embedded peptidomimetic scaffolds

To materialize this concept, we employed a computer-aided approach for the rational design of peptidomimetic scaffolds. First, we virtually constructed tricyclic scaffolds by integrating pyrimidodiazepine with an additional ring in varying sizes (3, 4, 5, and 6) and all possible

stereoisomers at each C_{sp3} junction, resulting in 41 geometrically distinct tricycles serving as potential peptidomimetic core skeletons (**Figure 3A**). Subsequently, we analyzed the structural characteristics of three pivotal protein secondary structures—β-turn, β-strand, and α-helix—focusing on the Cα centers where amino acid residues attach in order to identify suitable scaffolds. Once suitable candidates were identified, we refined the scaffolds to minimize geometric deviations and accommodate the decoration with amino acid residues. Three peptidomimetic scaffolds (**1**–**3**) corresponding to the β-turn, β-strand, and α-helix secondary structures were systematically derived from a single pyrimidodiazepine skeleton (**Figure 3B**).

Conformational analysis was carried out to validate the suitability of each selected peptidomimetic scaffold (**1**–**3**) in maintaining its native form[29]. This assessment was crucial as excessively flexible structures would fail to preserve their original conformations, thereby rendering them ineffective in mimicking the intended secondary structures. We investigated the diversity of conformations within the energy window (<2.8 kcal/mol), allowing the free rotation of bonds at ambient temperature[30,31]. Our designed scaffolds **1**, **2**, and **3** exhibited four, three, and seven possible conformers, respectively, while the tri-peptide backbone had 10 conformers. Upon overlaying the potential conformers, our scaffolds displayed minimal changes in the backbone structure and Cα position, contrasting with the linear peptide where rotation was unrestricted, leading to complete chain orientation reversal. Furthermore, we compared the structural disparities among possible conformers. Our scaffolds demonstrated low root mean square deviation (RMSD) values among the conformers, ranging from 0.01 to 0.72 Å, indicating preservation of the originally designed conformation, while the linear peptides exhibited high RMSD values up to 7.568 Å, lacking conformational consistency (**Figures 3C, S1**, and **Tables S1, S2**).

To validate the selected peptidomimetic scaffolds (**1**–**3**, **Figures 4** and **S2**), we conducted a rigorous *in silico* analysis using their energy-minimized conformers and actual crystal structures of PPIs available in the PDB. Since amino acid residues primarily participate in protein binding events, our analysis focused on the Cα center, the starting point of side-chain residues[32]. By comparing the Cα–Cα distances on the protein surface to those of our peptidomimetic scaffolds, we verified whether our scaffolds could accurately display the side-chain residues similarly to actual protein secondary structures in three-dimensional space. Additionally, we overlaid our scaffolds with crystal structures of representative proteins exhibiting each secondary structure, calculating RMSD values based on Cα distances between the protein crystal structures and our peptidomimetic scaffolds to confirm their structural similarity.

In the first case, we focused on the β-turn structure, which plays a crucial role in connecting and stabilizing protein tertiary structures, distinguished by its flexibility compared to other secondary structures[33]. Employing a computer-aided algorithm tailored to β-turn structural characteristics, we integrated binding residues or hot spot residues found in representative peptides into our designed scaffold. After obtaining the energy-minimized conformer of our β-turn mimetic scaffold **1**, we compared the distances between the Cα centers *i*, *i+1*, and *i+2* of scaffold **1** with those in actual β-turn peptides sourced from the PDB. The comparison revealed a consistent spatial occupancy between scaffold **1** and the actual peptide, Tryptophan zipper 1 (PDB:1le0) (**Figure 4A**). Superimposing scaffold **1** with the β-turn peptide further confirmed its backbone structure and the orientation of amino acid residues, yielding excellent RMSD values. This precise spatial mimicry is crucial for recognition events in PPIs.

Similarly, we identified the pyrimidodiazepine-containing tricycle **2** as a promising scaffold for mimicking the β-strand structure, characterized by alternating amino acid residues along a planar peptide surface[34]. Inspired by this structural feature, we designed scaffold **2** to alternate the orientation of amino acid side chains up, down, and up positions. Upon obtaining the energy-minimized conformer of the β-strand mimetic scaffold **2**, we introduced the hot spot residue of PD-1, a representative β-strand peptide[35], and compared their Cα–Cα distances. This comparison revealed a comparable scale of spatial occupancy between scaffold **2** and the PD-1 model peptide (**Figure 4B**). Overlaying scaffold **2** with the hot spot sequence of the PD-1 peptide demonstrated potential mimicry with an RMSD value of 0.810 Å. Additionally, we achieved excellent alignment in the orientation of amino acid residues with favorable RMSD values for other β-strand peptides in the PDB, affirming its suitability as a scaffold for mimicking the β-strand structure.

Lastly, our focus turned to utilizing the pyrimidodiazepine-containing tricycle to emulate the α-helix structure, where side chain residues typically reside on one face of the helix at positions *i*, *i+3* or *i+4*, *i+7* [13]. Our α-helix mimetic scaffold **3** exhibited favorable distances between the Cα centers of scaffold **3** and the Cα positions of α-helix peptide (**Figure 4C**). Additionally, the energy-minimized conformer of scaffold **3** exhibited commendable overlays and reasonable RMSD values of approximately 1 Å with natural α-helices in the PBD[35,36].

Systematic synthetic strategies for each scaffold

Our *in-silico* analysis clearly demonstrated that the pyrimidodiazepine-containing scaffolds **1**, **2**, and **3** effectively mimic the three pivotal protein secondary structures: β-turn, β-strand, and α-helix, respectively. These scaffolds can adopt the spatial orientations of hot spot residues with various R_1, R_2, and R_3 substituents on the polar and rigid polyheterocycles,

facilitating direct comparison of three distinct scaffolds systematically derived from a single pyrimidodiazepine skeleton, targeting three distinct secondary structures—a feature previously unattainable in peptidomimetics research.

In our efforts to streamline the synthesis of peptidomimetic scaffolds inspired by protein secondary structures, retrosynthetic analysis guided our strategy. Since the three scaffolds share a single pyrimidodiazepine core structure, we devised a coupling approach involving various diamine building blocks (**4**–**6**) with a single starting material, 4,6-dichloropyrimidine-5-carboxaldehyde (**Scheme 1A**). Unique chiral tri-amine building blocks (**5** and **6**) were designed and synthesized to efficiently access the β-strand (**2**) and α-helix mimetic scaffolds (**3**), respectively. These building blocks featured orthogonally protected nucleophilic functional groups to facilitate subsequent functionalization. The synthetic pathway for each mimetic scaffold incorporated key reactions such as nucleophilic aromatic substitution reaction (S_NAr) and intramolecular reductive amination for pyrimidodiazepine's 7-membered ring formation. Leveraging similar reaction mechanisms, this synthetic strategy enabled the efficient preparation of β-turn, β-strand, and α-helix mimetic scaffolds, each adorned with various R_1, R_2, and R_3 substituents. Each diamine (**4**–**6**) underwent S_NAr reaction with the single starting material, yielding the intermediate **7**, **10**, and **13** after introducing the R_1 group. Subsequently, the resulting intermediates cyclized *via* one-pot amine deprotection and reductive amination, resulting in each scaffold **8**, **11**, and **14** sharing the common pyrimidodiazepine core. Further steps involved the insertion of additional R_2 and R_3 substituents to produce the desired peptidomimetic scaffolds (**1**–**3**) decorated with amino acid residues (**Scheme 1B**, see **SI, General procedures 1–4** for details). Despite commencing with a single starting material, the unique nature of pyrimidine as a building block allowed the creation of three distinctive scaffolds, each following a similar synthetic pathway.

Structural proof and chemoinformatic analysis

As previously emphasized, our innovative design strategy emphasized the nitrogen-rich polar nature of our peptidomimetic core scaffolds to accommodate hydrophobic substituents effectively. Unlike previous individual secondary structure mimetic scaffolds, our three distinct scaffolds (**1**–**3**), representing three major protein secondary structures, effortlessly accommodate a range of hydrophobic substituents like Phe, Leu, Trp, commonly found in PPI hot spot interfaces[37] without compromising the drug-likeness, water solubility, and cell permeability. Furthermore, our devised scaffolds enable the functionalization of hot spot residues in a defined orientation on the rigid α-helix, β-strand, and β-turn mimetic frameworks.

To demonstrate the feasibility of our synthetic approach, we aimed to synthesize a representative library comprising three sets of 18 each, totaling 54 compounds for β-turn (**1a**–**1r**), β-strand (**2a**–**2r**), and α-helix (**3a**–**3r**) mimetic compounds, each featuring identical substituents at the R_1, R_2, and R_3 positions (**Figures 5A–C**). However, the different electronic nature of the ether groups on α-helix mimetics **3** limited the introduction of electron-push and pull moieties. The attempted introduction of an indole group, identical to the tryptophan amino acid residue, led to an immediate decomposition of the desired mimetic compounds during silica-gel flash column chromatography. For other mimetic scaffolds **1** and **2**, the tryptophan residue was either linked to the aniline position or an amide, thus avoiding spontaneous decomposition, unlike α-helix mimetics **3**. As a workaround, we introduced an *N*-protected indole at the R_1 position instead of R_3, subsequently removing the protection group. Even though we observed their partial degradation after approximately two weeks, we were able to utilize them for biological testing by immediate *N*-deprotection.

The three-dimensional structures of our peptidomimetic scaffolds (**1**–**3**) were unambiguously confirmed by single-crystal X-ray crystallography. We obtained crystal structures of **1s**, **2s**, and **3s**, representative compounds of each scaffold, to confirm that our synthesized peptidomimetic scaffolds accurately mimic the three pivotal secondary structures by comparing their Cα–Cα distances and RMSD values with those in real secondary structures in the PDB. Specifically, the crystal structures of **1s**, **2s**, and **3s** revealed similar Cα–Cα distances comparable to the representative peptides—Trp zipper 1 (PDB:1le0), PD-1 (PDB:4ZQK), and Bim (PDB:1PQ1), respectively, for each secondary structure—with their RMSD values within a narrow range of 0.690 Å, 0.717 Å, and 0.632 Å, respectively (**Figure 5D, TableS3**). This observation validated the successful mimicry of our synthesized scaffolds for peptidomimetics of three pivotal secondary structures, echoing our *in-silico* analysis with the energy-minimized conformer of each scaffold.

Traditional FDA-approved drugs typically target narrow, well-defined cavities within enzyme active sites or receptors, adhering to Lipinski's rule of five in most cases[1,38]. However, PPIs present a contrasting scenario characterized by broader, flatter, and more hydrophobic interfacial surfaces. This distinction prompted us to design PPI modulators with specific properties, such as increased hydrophobicity (higher cLogP values), elevated molecular weight, and enhanced hydrogen bonding capabilities[3]. To assess the suitability of our pyrimidodiazepine-based peptidomimetic compounds as valuable tools for systematic evaluation of PPI modulators, we conducted principal component analysis (PCA) using various molecular descriptors, including molecular weight, cLogP value, number of hydrogen bonding donor/acceptors, topological polar surface area, and number of rotatable bonds, as variables (**Figure 5E**). Our data strongly indicates that our peptidomimetic compounds (red)

possess properties conducive to PPI modulation (blue) while retaining drug-like characteristics akin to traditional FDA-approved drugs (yellow), unlike previously reported peptidomimetic compounds (navy) remaining only in the space of PPI modulator (blue). Hence, our peptidomimetic compound library holds promise as a valuable resource for addressing unmet medical needs, particularly as PPI modulators with drug-like properties

Biological evaluation

As depicted in **Figures 5A–C**, our peptidomimetic compound library comprises three sets of compounds, each featuring identical amino acid substituents but varying central scaffolds. Consequently, we anticipated distinct patterns of biological activities dependent on their respective scaffolds. To evaluate our hypothesis, we conducted two types of cell-based phenotypic screening, assessing the inhibitory effects on tau aggregation[39] and lipid droplets (LD) accumulation[40]. Our selection of disease-related phenotypes stems from the urgent therapeutic need to address neurodegenerative diseases, notably Alzheimer's disease (AD), associated with aging. Aβ and tau protein aggregation play pivotal roles in AD pathology, with tau aggregation emerging as a prominent therapeutic target[41–43]. Simultaneously, LDs, acting as lipid storage centers, are implicated in various biological events. While cells delicately maintain lipid metabolism through LD biogenesis, dysregulated LD accumulation is linked to metabolic syndromes and autophagy, a cellular recycling mechanism involved in protein aggregation-mediated neurodegenerative disorders[44–46]. The discovery of molecules targeting tau aggregation and LD accumulation holds promise for uncovering diverse biological pathways and offering therapeutic strategies for neurodegenerative diseases.

Through our cell-based phenotypic screenings, we observed diverse biological activities dependent on scaffolds. Using HEK293 human embryonic kidney cells with stable expression of Venus-based bimolecular fluorescence-complemented (BiFC)-tau, we assessed the cellular aggregation of tau under endoplasmic reticulum (ER) stress induced by thapsigargin (TG)[43,47]. Notably, the α-helix mimetic compounds **3a**, **3b**, and **3d** significantly inhibited tau aggregation induced by TG treatment in the BiFC-tau assay system (**Figure 6A**). These compounds displayed stronger inhibition effects on tau aggregation than the corresponding β-turn and β-strand compounds with identical amino acid substituents. Particularly, **3d** exhibited a notable inhibition effect on BiFC-tau Venus fluorescence (IC_{50} 1.21 μM) compared to **1d** and **2d** (**Figures 6B** and **S4A**). In parallel, our LD screenings with a fluorogenic LD probe SF44 in HeLa human cervical cancer cells revealed a significant reduction in cellular LDs upon treatment with the β-strand mimetic compounds **2a**, **2b**, and **2d**. These compounds exhibited

stronger inhibition effects on cellular LDs than the corresponding β-turn and α-helix compounds with identical amino acid substituents (**Figure 6A**). For instance, **2a** significantly reduced cellular LDs (IC_{50} 2.26 μM) compared to **1a** and **3a** (**Figures 6C** and **S4B**).

These findings underscore how distinct peptidomimetic scaffolds can yield different biological activities despite featuring identical amino acid residues. This emphasizes the versatility of our pyrimidodiazepine-derived peptidomimetic scaffolds in selectively modulating biological processes, particularly PPIs. Furthermore, our representative peptidomimetic compounds demonstrated low cytotoxicity at 10 μM across various cell lines, including HeLa cells, Raw264.7 murine macrophage cells, and C2C12 mouse myoblast cells (**Figure S4E**).

Conclusion

PPIs represent highly selective interactions crucial for regulating cellular behavior, making them vital targets in chemical biology and drug discovery. However, despite the estimated 650,000 interactomes in humans, only a tiny fraction of PPIs have been extensively studied[48,49]. Novel PPI modulators hold significant promise as therapeutic candidates or probing agents to explore unknown pathological PPIs. Unlike traditional drug targets, PPI interfaces lack distinct binding cavities and have been deemed undruggable. Peptides and selective antibodies, although explored for targeting PPIs, suffer from inherent limitations such as poor cell permeability and pharmacokinetics[50]. Overcoming these challenges requires employing small molecules with drug-like properties and robust pharmacokinetic profiles. However, small molecule-based peptidomimetics have been underutilized due to their inability to efficiently cover large PPI interfacial areas. Discovering substances that regulate the vast PPI family without rational design is time-consuming and labor-intensive, highlighting the need for novel, efficient strategies.

Despite the vast surface area of PPIs, hot spots where most of the binding energy is concentrated exist, offering the potential for exploring unknown PPIs and discovering PPI modulators. Our study proposes a novel rational design strategy, overcoming limitations inherent in conventional peptides. We readily created scaffolds mimicking the three major protein secondary structures by employing the same reaction mechanism on a single core skeleton, pyrimidodiazepine. This generic approach, covering the three major secondary structure elements, holds promise for offering a broader spectrum of PPI modulators with drug-like properties to overcome the limitations of traditional peptidomimetic approaches. Recognizing the significance of uncovering unexplored PPIs and the promise of nonpeptidic scaffolds mimicking different protein secondary structures, we envision our pyrimidodiazepine-

derived peptidomimetic scaffolds as a valuable resource in chemical biology and drug discovery.

Methods

Synthetic procedures

All synthetic procedures are provided in Supplementary Information. X-ray crystallographic image and data of compound **S10**, **1s**, **2s**, and **3s** are reported in Supplementary Figure S2, Table S3. The CCDC deposition numbers 2353935 (for **1s**), 2353936 (for **3s**), 2353937 (for **2s**), and 2353938 (for **S10**). These data are provided free of charge by the joint Cambridge Crystallographic Data Centre and Fachinformationszentrum Karlsruhe Access Structures service.

Computational methods

All quantum mechanical calculations were performed in Gaussian09W. The ground state structures were optimized using density functional theory (DFT) at the B3LYP/6-31G(d) level. All protein crystal structures were obtained from the protein data bank (PDB). The visualization of molecules and the superimposition with protein crystal structures were performed using Discovery Studio. Our scaffold and protein Cα were overlapped, and the distance between them was obtained and used to calculate RMSD. Principal component analysis (PCA) was performed using R.Studio, iPPi database was used for 2246 PPI modulators (2023 February updated), and eDrug 3D database was used for 1596 FDA approved drugs (~2023 June accepted). The chemical properties used in the PCA are molecular weight, cLogP value, number of hydrogen bonding donor/acceptors, topological polar surface area, and number of rotatable bonds.

Cell culture

HeLa human cervical cancer cells were cultured in RPMI with 10% (v/v) FBS and 1% AA solution. BiFC-tau stable HEK293 human embryonic kidney cells were cultured in DMEM with 10% FBS, 1% (v/v) AA solution, and Geneticin (100 μg/mL). Raw264.7 murine macrophage cells and C2C12 murine myoblast cells were cultured in DMEM with 10% (v/v) FBS and 1% (v/v) AA solution. Cells were maintained in a 100-mm cell culture dish in an incubator at 37°C under a humidified atmosphere with 5% CO_2.

Tau aggregation screening using BiFC-tau Venus HEK293 cell

BiFC-tau HEK293 cells were seeded into black 384-well plates at a density of 7×10^4 cells/well in 40 μL media for 24 h. Compounds were treated with 80 nM thapsigargin in 10 uL media. After 24 h, nuclei were stained by Hoechst 33342 for 10 min. Plates were scanned in an InCell Analyzer 2500 at $\lambda_{ex}/\lambda_{em}$ =490/525 nm (for FITC channel) for Venus fluorescence and at $\lambda_{ex}/\lambda_{em}$=350/455 nm (for DAPI channel) for nuclei. Obtained images were analyzed to quantify Venus fluorescence intensity per cell using InCell Developer software.

Lipid droplet screening with SF44

HeLa cells were seeded into black 96-well plates at a density of 4×10^4 cells/well in 100 μL media. After 24 h, the compounds were treated. Oleic acid (10 μM) and serum-free RPMI were used as a positive and negative control, respectively. Due to the cytotoxicity, serum-free RPMI was treated for 20 h. After incubation, SF44 was treated to each well in a final concentration of 5 μM for 20 min, followed by Hoechst 33342 staining for an additional 10 min. Plates were scanned in an InCell Analyzer 2500 at $\lambda_{ex}/\lambda_{em}$=430/605 nm (for FITC channel) for SF44 fluorescence on lipid droplets and at $\lambda_{ex}/\lambda_{em}$=350/455 nm (for DAPI channel) for nuclei. The images obtained were analyzed using InCell Developer software. The fluorescence intensity of LDs was interpreted as a cellular granule, and the area of individual cells was recognized by nuclei staining with collar segmentation.

Cell Viability assay

HeLa human cervical cancer cells, Raw264.7 murine macrophage cells, and C2C12 murine myoblast cells were seeded in transparent 96-well plates. After 24 h, compounds were treated at a concentration of 10 μM for 24 h. Then, a cell viability assay was performed with a WST assay following the manufacturer's protocol.

Data availability

The data that support the findings of this study are available in the Supplementary Information of this article.

References

1. Lu, H. *et al.* Recent advances in the development of protein–protein interactions modulators: mechanisms and clinical trials. *Signal Transduct. Target. Ther.* **5**, (2020).
2. Ran, X. & Gestwicki, J. E. Inhibitors of protein–protein interactions (PPIs): an analysis of scaffold choices and buried surface area. *Curr. Opin. Chem. Biol.* **44**, 75–86 (2018).

3. Shin, W. H., Kumazawa, K., Imai, K., Hirokawa, T. & Kihara, D. Current challenges and opportunities in designing protein–protein interaction targeted drugs. *Adv. Appl. Bioinforma. Chem.* **13**, 11–25 (2020).
4. Zhao, L., Zhao, J., Zhong, K., Tong, A. & Jia, D. Targeted protein degradation: mechanisms, strategies and application. *Signal Transduct. Target. Ther.* **7**, (2022).
5. Békés, M., Langley, D. R. & Crews, C. M. PROTAC targeted protein degraders: the past is prologue. *Nat. Rev. Drug Discov.* **21**, 181–200 (2022).
6. Cho, W. *et al.* Targeted Protein Upregulation of STING for Boosting the Efficacy of Immunotherapy. *Angew. Chem. Int. Ed.* **62**, e202300978 (2023).
7. Chen, S. Y. & Zacharias, M. What Makes a Good Protein-Protein Interaction Stabilizer: Analysis and Application of the Dual-Binding Mechanism. *ACS Cent. Sci.* **9**, 969–979 (2023).
8. Azzarito, V., Long, K., Murphy, N. S. & Wilson, A. J. Inhibition of α-helix-mediated protein-protein interactions using designed molecules. *Nat. Chem.* **5**, 161–173 (2013).
9. Shin, W. H., Kumazawa, K., Imai, K., Hirokawa, T. & Kihara, D. Current challenges and opportunities in designing protein–protein interaction targeted drugs. *Adv. Appl. Bioinforma. Chem.* **13**, 11–25 (2020).
10. Lenci, E. & Trabocchi, A. Peptidomimetic toolbox for drug discovery. *Chem. Soc. Rev.* **49**, 3262–3277 (2020).
11. Guo, W., Wisniewski, J. A. & Ji, H. Hot spot-based design of small-molecule inhibitors for protein-protein interactions. *Bioorganic Med. Chem. Lett.* **24**, 2546–2554 (2014).
12. Monteleone, S. *et al.* Hotspot Identification and Drug Design of Protein-Protein Interaction Modulators Using the Fragment Molecular Orbital Method. *J. Chem. Inf. Model.* **62**, 3784–3799 (2022).
13. Pelay-Gimeno, M., Glas, A., Koch, O. & Grossmann, T. N. Structure-Based Design of Inhibitors of Protein-Protein Interactions: Mimicking Peptide Binding Epitopes. *Angew. Chem. Int. Ed.* **54**, 8896–8927 (2015).
14. Gokhale, A. S. & Satyanarayanajois, S. Peptides and peptidomimetics as immunomodulators. *Immunotherapy* **6**, 755–774 (2014).
15. Tošovská, P. & Arora, P. S. Oligooxopiperazines as nonpeptidic α-helix mimetics. *Org. Lett.* **12**, 1588–1591 (2010).
16. Lao, B. B. *et al.* Rational design of topographical helix mimics as potent inhibitors of protein-protein interactions. *J. Am. Chem. Soc.* **136**, 7877–7888 (2014).
17. Orner, B. P., Ernst, J. T. & Hamilton, A. D. Toward proteomimetics: Terphenyl derivatives as structural and functional mimics of extended regions of an α-helix [18]. *J. Am. Chem. Soc.* **123**, 5382–5383 (2001).
18. Yin, H. *et al.* Terphenyl-based helical mimetics that disrupt the p53/HDM2 interaction. *Angew. Chem. Int. Ed.* **44**, 2704–2707 (2005).
19. Angelo, N. G. & Arora, P. S. Solution- and solid-phase synthesis of triazole oligomers that display protein-like functionality. *J. Org. Chem.* **72**, 7963–7967 (2007).
20. Jochim, A. L., Miller, S. E., Angelo, N. G. & Arora, P. S. Evaluation of triazolamers as active site inhibitors of HIV-1 protease. *Bioorganic Med. Chem. Lett.* **19**, 6023–6026 (2009).
21. Wyrembak, P. N. & Hamilton, A. D. Alkyne-linked 2,2-disubstituted-indolin-3-one oligomers as extended β-strand mimetics. *J. Am. Chem. Soc.* **131**, 4566–4567 (2009).

22. Whitby, L. R. *et al.* Design, synthesis, and validation of a β-turn mimetic library targeting protein - Protein and peptide - Receptor interactions. *J. Am. Chem. Soc.* **133**, 10184–10194 (2011).

23. Kim, C., Jung, J., Tung, T. T. & Park, S. B. β-Turn mimetic-based stabilizers of protein-protein interactions for the study of the non-canonical roles of leucyl-tRNA synthetase. *Chem. Sci.* **7**, 2753–2761 (2016).

24. Kim, J., Kim, H. & Park, S. B. Privileged structures: Efficient chemical 'navigators' toward unexplored biologically relevant chemical spaces. *J. Am. Chem. Soc.* **136**, 14629–14638 (2014).

25. Kim, J. *et al.* Diversity-oriented synthetic strategy for developing a chemical modulator of protein-protein interaction. *Nat. Commun.* **7**, 1–10 (2016).

26. Nammalwar, B. & Bunce, R. A. Recent Advances in Pyrimidine-Based Drugs. *Pharmaceuticals* **17**, (2024).

27. Gracias, V. *et al.* Scaffold oriented synthesis. Part 2: Design, synthesis and biological evaluation of pyrimido-diazepines as receptor tyrosine kinase inhibitors. *Bioorganic Med. Chem. Lett.* **18**, 2691–2695 (2008).

28. Smith, M. C. & Gestwicki, J. E. Features of protein-protein interactions that translate into potent inhibitors: topology, surface area and affinity. *Expert Rev. Mol. Med.* **14**, 1–20 (2012).

29. Ko, E., Liu, J. & Burgess, K. Minimalist and universal peptidomimetics. *Chem. Soc. Rev.* **40**, 4411–4421 (2011).

30. Erickson, L. E. & Morris, K. F. The energy profile for rotation about the C-C bond in substituted ethanes: A multi-part experimental and computational project for the physical chemistry laboratory. *J. Chem. Educ.* **75**, 900–906 (1998).

31. Liu, C., Wang, Y., Zhao, D. xia, Gong, L. dong & Yang, Z. zhi. Development of ABEEMσπ polarizable force field for oxidized adenine base pairs: investigation of the interaction and mutagenic mechanism. *Theor. Chem. Acc.* **133**, 1–14 (2014).

32. Conte, L. Lo, Chothia, C. & Janin, J. The atomic structure of protein-protein recognition sites. *J. Mol. Biol.* **285**, 2177–2198 (1999).

33. Gibbs, A. C., Bjorndahl, T. C., Hodges, R. S. & Wishart, D. S. Probing the structural determinants of type II′ β-turn formation in peptides and proteins. *J. Am. Chem. Soc.* **124**, 1203–1213 (2002).

34. Watkins, A. M. & Arora, P. S. Anatomy of β - Strands at Protein − Protein Interfaces. *ACS Chem. Biol.* **9**, 1747–1754 (2014).

35. Yin, H. *et al.* Rational Design of Potent Peptide Inhibitors of the PD-1:PD-L1 Interaction for Cancer Immunotherapy. *J. Am. Chem. Soc.* **143**, 18536–18547 (2021).

36. Abdildinova, A. & Gong, Y. D. Traceless solid-phase synthesis and β-turn propensity of 1,3-thiazole-based peptidomimetics. *RSC Adv.* **11**, 1050–1056 (2020).

37. Siegert, T. R., Bird, M. J., Makwana, K. M. & Kritzer, J. A. Analysis of Loops that Mediate Protein-Protein Interactions and Translation into Submicromolar Inhibitors. *J. Am. Chem. Soc.* **138**, 12876–12884 (2016).

38. Shultz, M. D. Two Decades under the Influence of the Rule of Five and the Changing Properties of Approved Oral Drugs. *J. Med. Chem.* **62**, 1701–1714 (2019).

39. Hernández, F. *et al.* Tau Aggregation. *Neuroscience* **518**, 64–69 (2023).

40. Olzmann, J. A. & Carvalho, P. Dynamics and functions of lipid droplets. *Nat. Rev. Mol. Cell Biol.* **20**, 137–155 (2019).
41. Grundke-Iqbal, I. *et al.* Abnormal phosphorylation of the microtubule-associated protein tau (tau) in Alzheimer cytoskeletal pathology. *Proc. Natl. Acad. Sci. U. S. A.* **83**, 4913–4917 (1986).
42. Congdon, E. E. & Sigurdsson, E. M. Tau-targeting therapies for Alzheimer disease. *Nat. Rev. Neurol.* **14**, 399–415 (2018).
43. Shin, Y. H. *et al.* Phenotypic Discovery of Neuroprotective Agents by Regulation of Tau Proteostasis via Stress-Responsive Activation of PERK Signaling. *Angew. Chem. Int. Ed.* **60**, 1831–1838 (2021).
44. Farmer, B. C., Walsh, A. E., Kluemper, J. C. & Johnson, L. A. Lipid Droplets in Neurodegenerative Disorders. *Front. Neurosci.* **14**, 1–13 (2020).
45. Zadoorian, A., Du, X. & Yang, H. Lipid droplet biogenesis and functions in health and disease. *Nat. Rev. Endocrinol.* **19**, 443–459 (2023).
46. Lee, S., Kim, E. & Park, S. B. Discovery of autophagy modulators through the construction of a high-content screening platform via monitoring of lipid droplets. *Chem. Sci.* **4**, 3282–3287 (2013).
47. Tak, H. J. *et al.* Bimolecular fluorescence complementation; Lighting-up tau-tau interaction in living cells. *PLoS One* **8**, 1–7 (2013).
48. Patil, S. P. Exploring Small Molecules Targeting Protein–Protein Interactions (PPIs): Advancements and Future Prospects. *Pharmaceuticals* **16**, 1–3 (2023).
49. Mabonga, L. & Kappo, A. P. Protein-protein interaction modulators: advances, successes and remaining challenges. *Biophys. Rev.* **11**, 559–581 (2019).
50. Nevola, L. & Giralt, E. Modulating protein-protein interactions: The potential of peptides. *Chem. Commun.* **51**, 3302–3315 (2015).

Acknowledgements

This work was supported by a National Creative Research Initiative Grant (2014R1A3A2030423) and University Research Institute in Science Technology grant (2019R1A6A1A1007343 7) through the National Research Foundation of Korea (NRF) funded by the Korean Government (MEST). This work was also supported by SPARK Biopharma research grant (SRnD 0409-20210245).

Author contributions

J.Y.Y., C. K., and S. B. P. conceived and designed the project. J.Y.Y., C.K., K.J., and W.P. performed chemical synthesis and characterization. J.Y.Y. and C.K. performed *in silico* analysis and density functional theory calculations and analyzed the experimental data. J.H.K. and H.C. performed phenotypic screening, cellular imaging, and cell viability test. Y.K. and D.L. obtained the XRD and solved the structures. J.Y.Y. and S.B.P. co-wrote the manuscript through

contributions from all other authors. All authors have given approval to the final version of the manuscript.

Competing interests

The authors declare no competing interests.

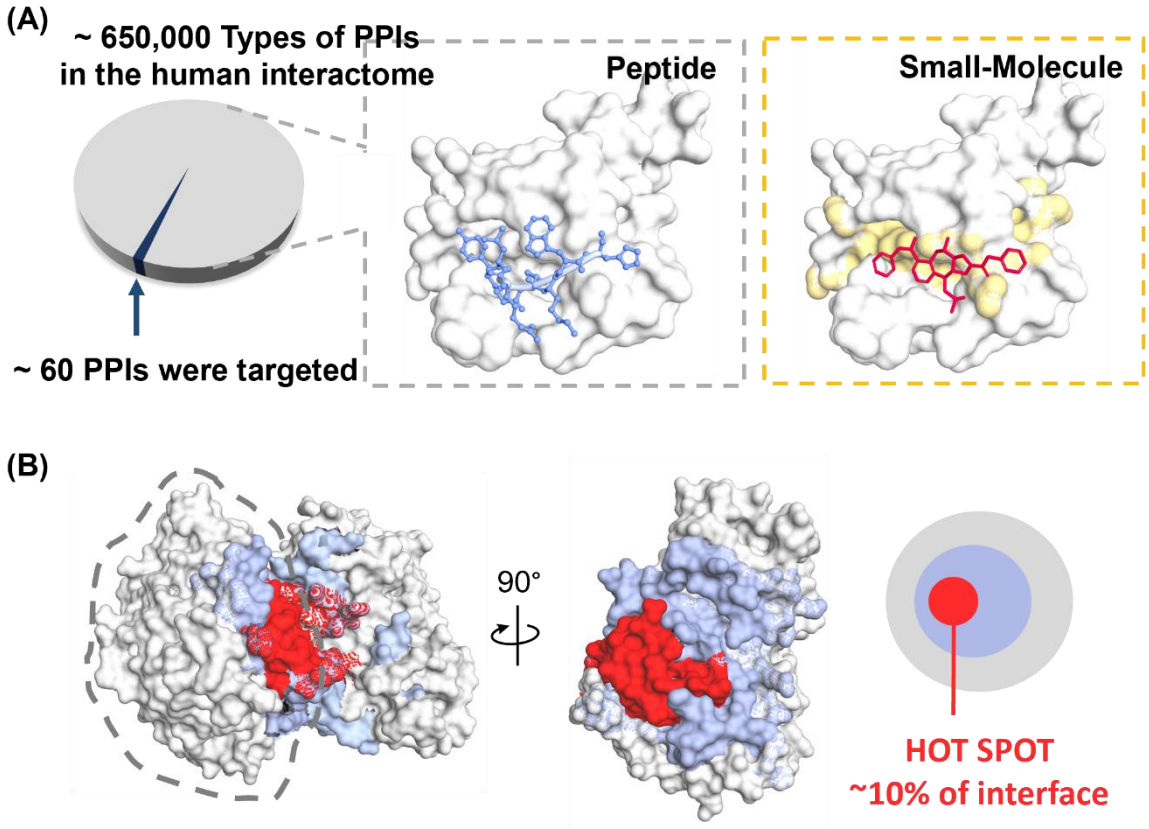

Figure 1. Current state of protein-protein interaction modulators. (A) Current state of PPI targeting (B) Interaction area of proteins and their hot spots.

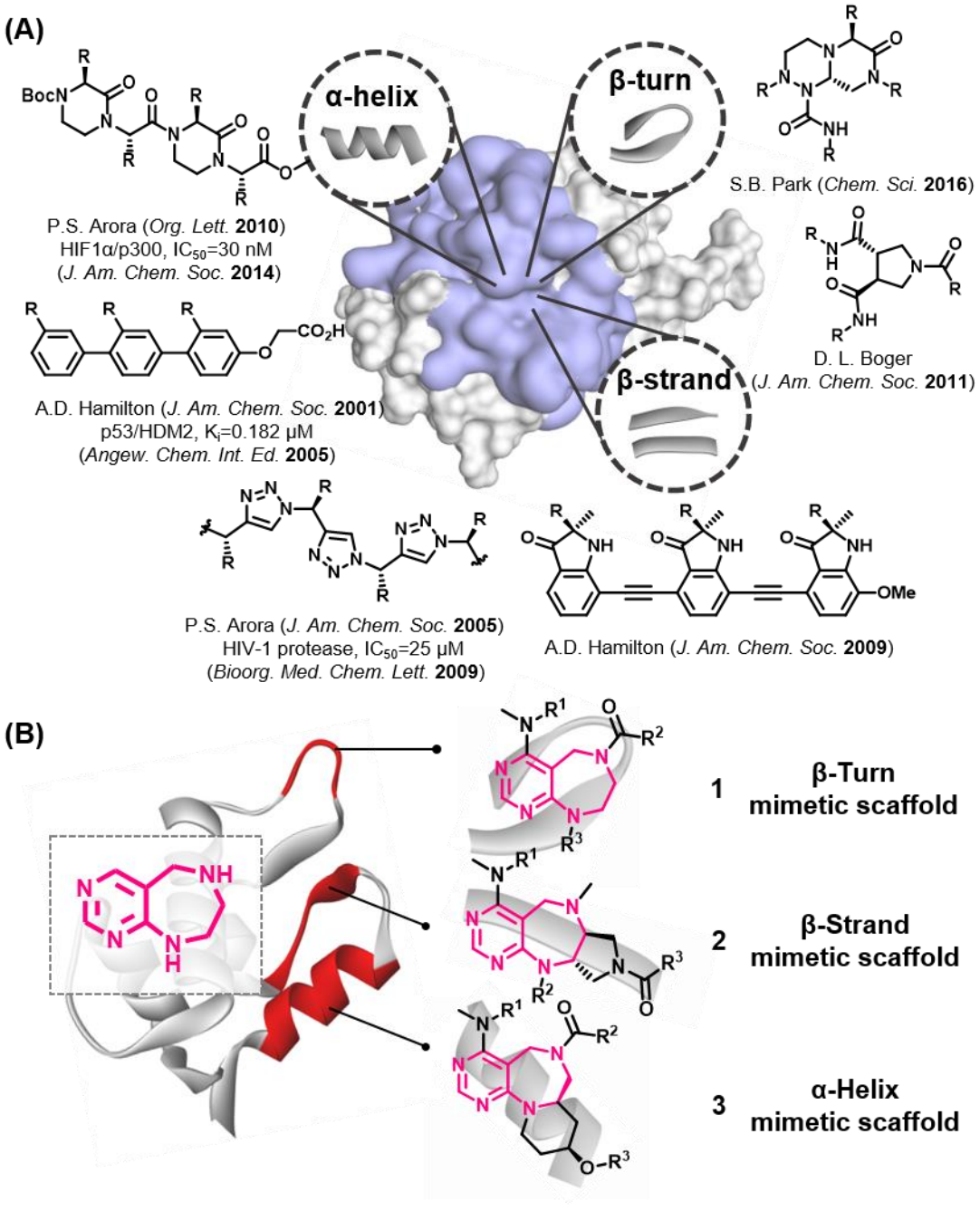

Figure 2. Small-molecule mimetics for three major secondary structures. (A) Examples of previously reported peptidomimetic scaffolds. (B) Novel pyrimidodiazepine-based peptidomimetic scaffolds.

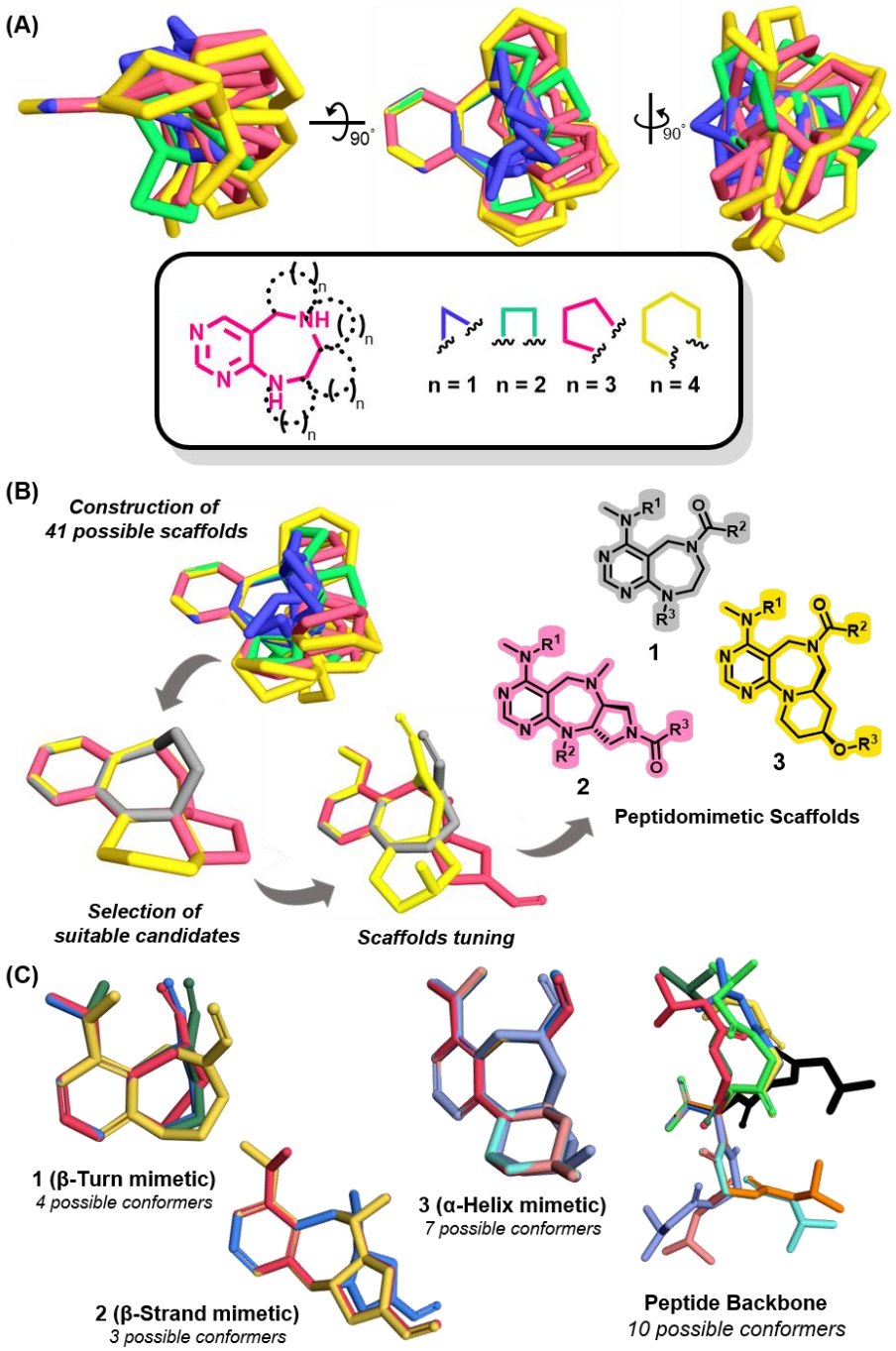

Figure 3. Selection of scaffold candidates. (A) Virtual construction of peptidomimetic scaffold candidates by fusing pyrimidodiazepine with an additional ring in varying sizes (3, 4, 5, and 6) and all possible stereoisomers. (B) Selection of appropriate peptidomimetic scaffolds (**1**–**3**) from virtually constructed 41 scaffolds. (C) Overlaid conformers for selected peptidomimetics scaffolds (**1**–**3**) and a linear tripeptide within the energy window (<2.8 kcal/mol) at ambient temperature.

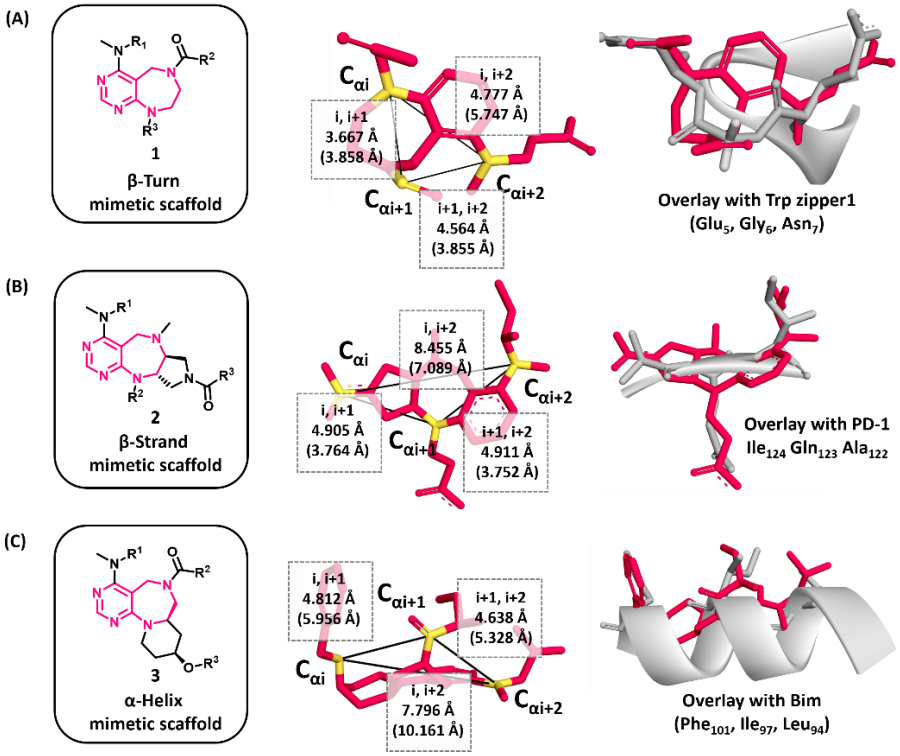

β-Turns	RMSD (Å)
Trp zipper1 (PDB:1le0)	0.585
TrxR (PDB:4B1B)	0.675
HC19 CDR L3 (PDB:1GIG)	0.584

β-Strands	RMSD (Å)
PD1-PD-L1 (PDB:4ZQK)	0.810
P65 Homodimer (PDB:1OY3)	0.793
Ras-Raf (PDB:1RRB)	0.745

α-Helices	RMSD (Å)
Bcl-xl/Bim (PDB:1PQ1)	0.977
Mcl-1/Bim BH3 (PDB:2NL9)	1.055
HIF-1α/p300 (PDB:1L8C)	1.007

Figure 4. Computer-aided design of secondary structure mimetics. Three novel scaffolds that mimic three major secondary structures are shown with the Cα–Cα distance, RMSD values by aligning Cα on the peptide with Cα equivalents on the mimetic scaffold, and alignment forms with representative peptides in the protein data bank (PDB). (A) In silico analysis of β-turn mimetic scaffold **1**; (B) In silico analysis of β-strand mimetic scaffold **2**; (C) In silico analysis of α-helix mimetic scaffold **3**.

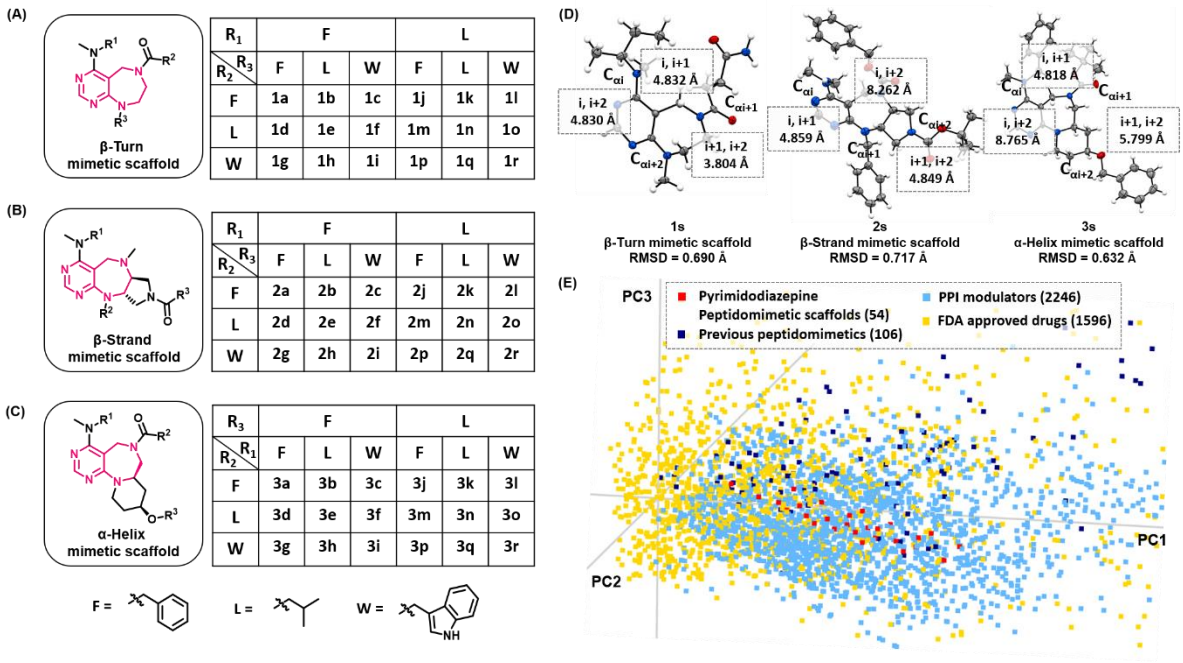

R_1 / R_2 R_3	F	L	W	F	L	W
F	1a	1b	1c	1j	1k	1l
L	1d	1e	1f	1m	1n	1o
W	1g	1h	1i	1p	1q	1r

R_1 / R_3 R_2	F	L	W	F	L	W
F	2a	2b	2c	2j	2k	2l
L	2d	2e	2f	2m	2n	2o
W	2g	2h	2i	2p	2q	2r

R_3 / R_1 R_2	F	L	W	F	L	W
F	3a	3b	3c	3j	3k	3l
L	3d	3e	3f	3m	3n	3o
W	3g	3h	3i	3p	3q	3r

Figure 5. Synthetic results of peptidomimetic library compounds that have diverse characteristics. (A) General structure and synthesized compounds of β-turn mimetics. (B) General structure and synthesized compounds of β-strand mimetics. (C) General structure and synthesized compounds of α-helix mimetic. (D) Single-crystal X-ray structures of **1s**, **2s**, and **3s** representing each peptidomimetic scaffolds and their structural comparison (Cα–Cα distance and RMSD value) with reported protein secondary structures—Trp zipper 1 (PDB:1le0), PD-1 (PDB:4ZQK), and Bim (PDB:1PQ1), respectively—in PDB. (E) Principal component analysis of our pyrimidodiazepine-based peptidomimetics library (red) with FDA approved drugs (yellow), PPI modulators (blue), and previously reported peptidomimetics (navy).

(A)

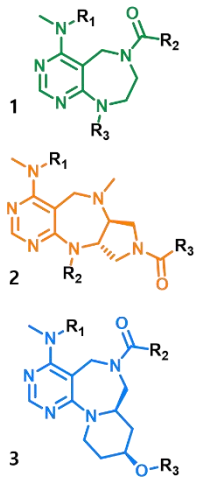

		R_1	R_2	R_3	Tau BiFC	Lipid droplet
					% inhibition at 10 μM (IC_{50})	% inhibition at 10 μM (IC_{50})
β-Turn mimetic scaffolds	**1a**	Bn (F)	Bn (F)	Bn (F)	43.8	-0.3
	1b	Bn (F)	Bn (F)	*i*-Bu (L)	40.6	4.1
	1d	Bn (F)	*i*-Bu (L)	Bn (F)	-11.8	-11.6
β-Strand mimetic scaffolds	**2a**	Bn (F)	Bn (F)	Bn (F)	50.0	**81.8 (2.26 μM)**
	2b	Bn (F)	Bn (F)	*i*-Bu (L)	8.6	**85.1 (2.47 μM)**
	2d	Bn (F)	*i*-Bu (L)	Bn (F)	-11.8	**71.2 (2.71 μM)**
α-Helix mimetic scaffolds	**3a**	Bn (F)	Bn (F)	Bn (F)	**81.3 (0.58 μM)**	14.6
	3b	Bn (F)	Bn (F)	*i*-Bu (L)	**75.1 (2.98 μM)**	13.0
	3d	Bn (F)	*i*-Bu (L)	Bn (F)	**77.3 (1.21 μM)**	14.7

(B)

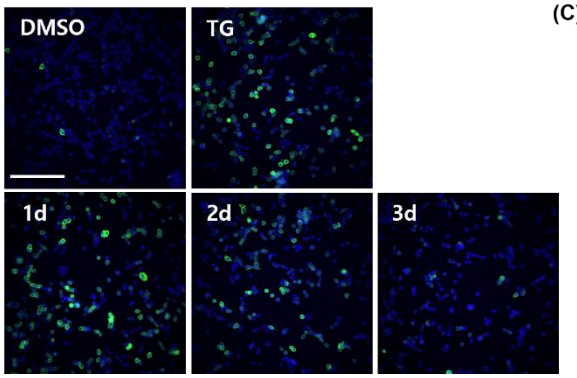

(C)

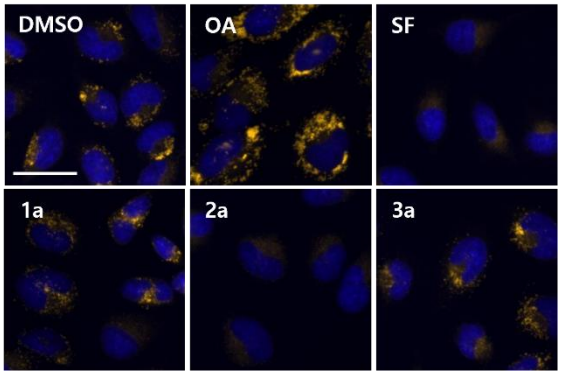

Figure 6. Biological activities of peptidomimetic compounds that show distinct features depending on their scaffolds. (A) The results of two kinds of disease-mimicking phenotypic assays for BiFC-tau and lipid droplets. (B) Representative images of BiFC-tau screening upon compound treatment (10 μM) in the presence of thapsigargin (TG, 80 nM). Scale bar = 200 μm. (C) Representative images of Lipid droplet screening upon compound treatment at 10 μM concentration with oleic acid (OA) and serum-free (SF) conditions as positive and negative controls, respectively. Scale bar = 30 μm. Data in (A) are average value of all replicated experiments, which have been repeated ≥ 3 times.

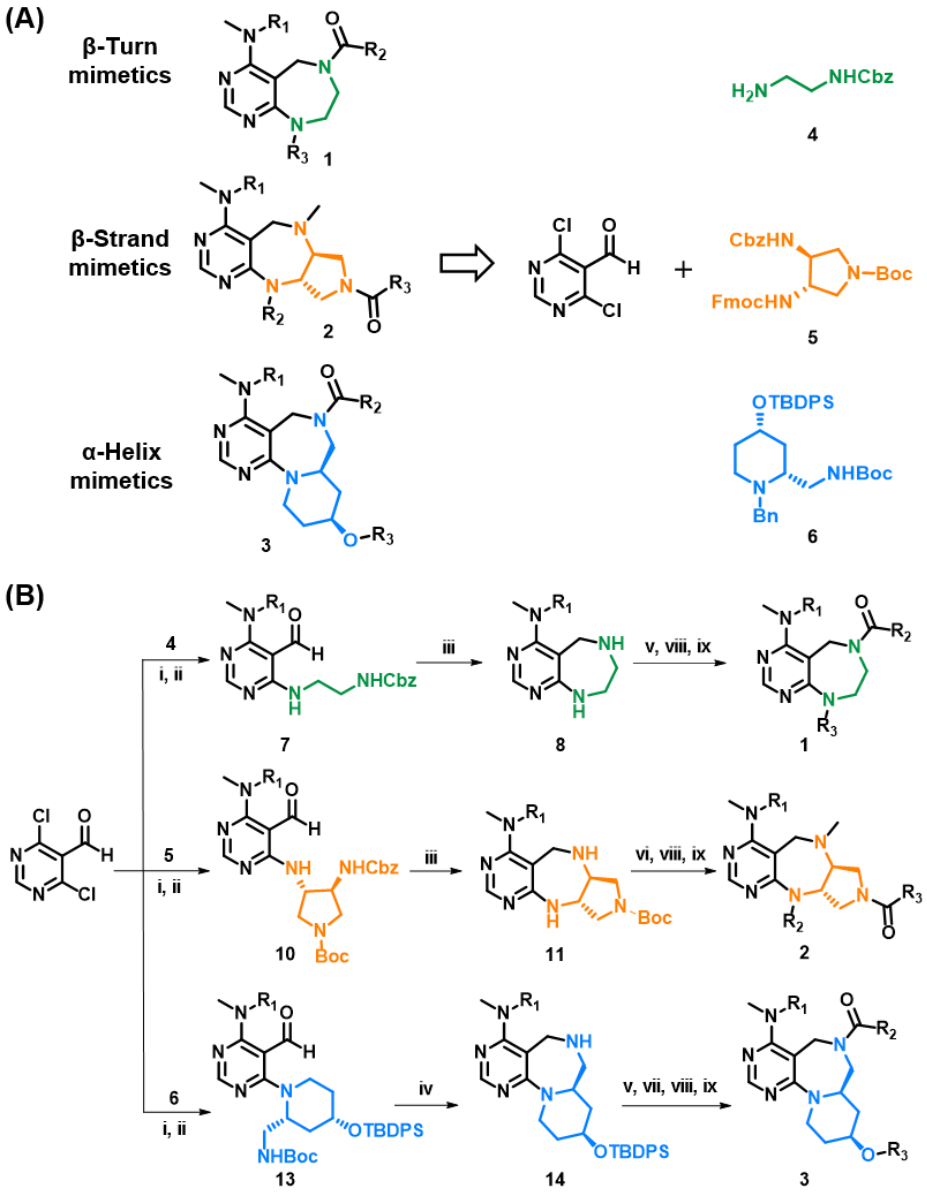

Scheme 1. Overall synthetic scheme for peptidomimetic scaffolds. (A) Retrosynthetic analysis with various chiral building blocks **4**–**6**. (B) Synthetic schemes of secondary mimetic scaffolds. Reagents and conditions: (i) TEA, chloroform, 0 °C to r.t.; (ii) Me-NH-R_1, K_2CO_3, DMF, 45 °C; (iii) Pd/C, H_2 (g), MeOH, r.t.; (iv) TFA, DCM, r.t., then $NaBH(OAc)_3$, DCE, 0 °C to r.t.; (v) Boc_2O, TEA, DCM, 0 °C; (vi) CH_3I, K_2CO_3, DMF, r.t.; (vii) TBAF, THF, r.t.; (viii) NaH, R_2-X or R_3-X, DMF, 0 °C to r.t.; (ix) TFA, DCM, r.t., then TEA, $R_3(CO)OSU$ or $R_2(CO)OSU$, DCM, r.t.

Table of Contents

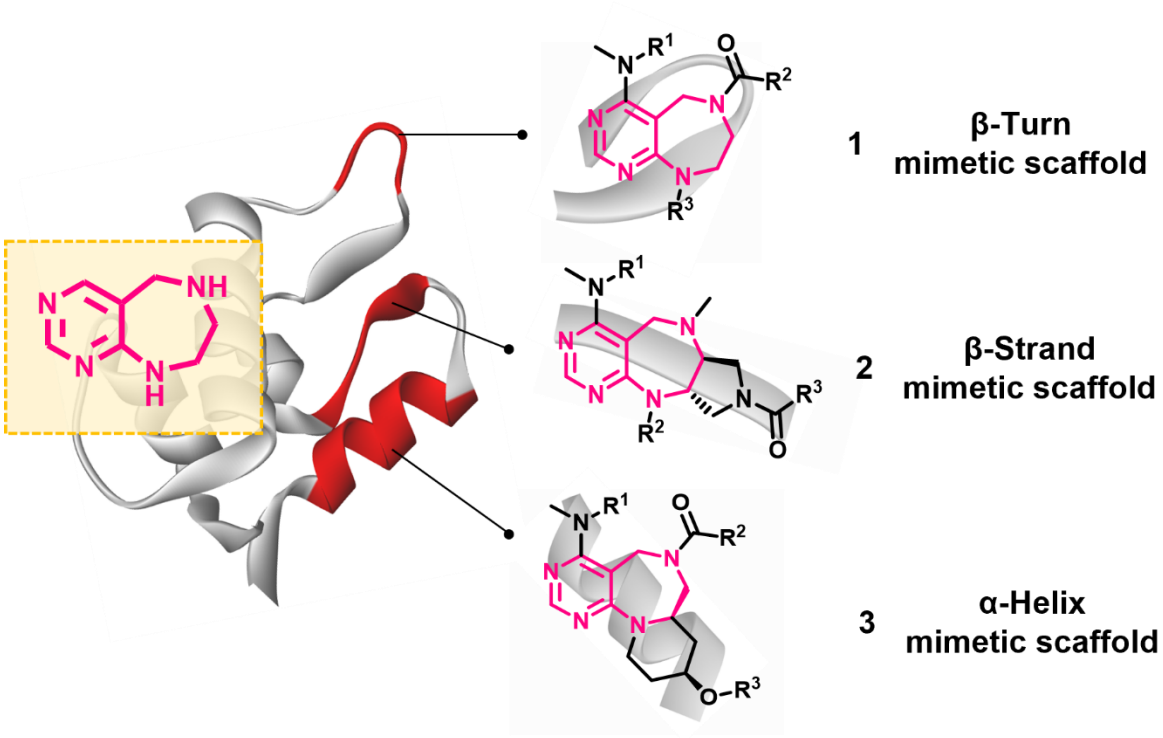

PPI modulators hold significant promise as therapeutic candidates or probing agents to explore unknown pathological PPIs. Herein, we introduced a computational method encompassing three essential secondary structures of peptidomimetic scaffolds—α-helix, β-strand, and β-turn—as key recognition motifs for protein-protein interfaces. These scaffolds (**1**–**3**), systematically derived from a single pyrimidodiazepine skeleton, offer a broader spectrum of PPI modulators with drug-like properties to overcome the limitations of traditional peptidomimetic approaches.